Journal of Alloys and Compounds 506 (2010) 210–215

Contents lists available at ScienceDirect

Journal of Alloys and Compounds

journal homepage: www.elsevier.com/locate/jallcom

Amorphization of equimolar alloys with HCP elements during mechanical alloying

Yu-Liang Chen[a,b], Che-Wei Tsai[b], Chien-Chang Juan[b], Ming-Hao Chuang[b], Jien-Wei Yeh[b,*], Tsung-Shune Chin[c], Swe-Kai Chen[d]

[a] Materials and Electro-Optics Research Division, Chung-Shan Institute of Science and Technology, Armaments Bureau, MND, P.O. Box 90008-8-5, Lung-Tan, Tao-Yuan 32599, Taiwan, ROC
[b] Department of Materials Science and Engineering, National Tsing Hua University, 101, Sec. 2, Kuang-Fu Road, Hsinchu 30013, Taiwan, ROC
[c] Department of Materials Science and Engineering, Feng Chia University, 100, Wenhwa Rd., Seatwen District, Taichung 40724, Taiwan, ROC
[d] Center for Nanotechnology, Materials Science and Microsystems, National Tsing Hua University, 101, Sec. 2, Kuang-Fu Road, Hsinchu 30013, Taiwan, ROC

ARTICLE INFO

Article history:
Received 19 February 2010
Received in revised form 23 June 2010
Accepted 30 June 2010
Available online 7 July 2010

Keywords:
Metals and alloys
Mechanical alloying
Phase evolution
Amorphization
High entropy alloy

ABSTRACT

This study prepares two equimolar alloys, entirely composed of HCP elements, BeCoMgTi and BeCoMgTiZn, from elemental powders by mechanical alloying. No crystalline solid solutions and compounds formed during milling except an amorphous phase formed gradually until full amorphization was attained. The amorphization processes of these two alloys conform to type II according to the Weeber and Bakker classification based on binary alloys. The inhibition of crystalline solid solutions and compounds before amorphization relates to chemical compatibility, high entropy effect and large atomic size difference effect.

1. Introduction

In 1970, Benjamin first developed mechanical alloying (MA) technique to fabricate oxide dispersion strengthened (ODS) iron- and nickel-based superalloys [1]. Since MA is a solid-state process, the difficulty in preparing alloys by melting elemental raw materials with large difference in melting point can be eliminated. In addition, the disadvantages induced in the liquid-to-solid process such as the unavoidable compositional segregation and negative eutectic or similar reactions can be prevented. Therefore, MA technique is versatile and have been extensively used to prepare a variety of materials such as amorphous alloy powders, nanocrystalline powders, intermetallic powders, composite and nanocomposite powders [2].

Among the research of MA, amorphization is one of the most frequently reported phenomena in MA powder mixtures [3]. Weeber and Bakker had classified the amorphization reactions of MA in binary alloys into three types in 1988 [4]. The first type (type I) featured peak shifting of each element due to formation of a crystalline solid solution phase, and then peak broadening due to the formation of amorphous structure. The second type (type II) featured a decrease of elemental peaks accompanied with an increase of the amorphous broad peak. The final type (type III) featured the formation of an intermetallic or intermediate compound prior to amorphous structure [4]. Recent research on multi-component amorphous alloys prepared by MA has revealed that their amorphization processes also fall into the three types: for example, type I in Zr–Ti–Cu–Ni [5] and Ni–Al–Ti [6], type II in Ti–Ni–Cu [7] and Al–Ni–Fe–Gd [8], and type III in Ni–Al–Ti–C [9] and Al–Cr–Co–Ce [10]. Nevertheless all these alloy systems are based on one principal metallic element whose content is higher than 50 at.%.

A high entropy alloy (HEA) is defined as having at least five principal elements in equimolar or near equimolar compositions [11]. Recently, various topics on HEAs have been reported, including microstructure and mechanical properties [12–14], effects of adding more elements [15,16], thermal stability [17–19], wear and corrosion resistance [20,21], hard coating [22,23], barrier films [24,25] and mechanical alloying behavior [26–30]. These are helpful in understanding HEAs in both academic and application aspects. Among these researches, it has been noted that HEAs prepared by melting method tend to form simple BCC and/or FCC solid solution phases due to high entropy effect and might possess a range of promising properties. However, for the HEA systems prepared by MA, such as Al–Fe–Ti–Cr–Zn–Cu [26],

* Corresponding author. Tel.: +886 35719558; fax: +886 35722366.
E-mail address: jwyeh@mx.nthu.edu.tw (J.-W. Yeh).

0925-8388/$ – see front matter © 2010 Elsevier B.V. All rights reserved.
doi:10.1016/j.jallcom.2010.06.179

Table 1
Fundamental properties of the experimental elements [31].

	Be	Co	Mg	Ti	Zn
Atomic size (Å)	1.13	1.25	1.60	1.46	1.39
Melting point (°C)	1289	1497	649	1673	419.7
a (Å)	2.27	2.51	3.21	2.95	2.66
c (Å)	3.59	4.07	5.21	4.68	4.95
c/*a* ratio	1.58	1.62	1.62	1.59	1.86

Cu–Ni–Al–Co–Cr–Fe–Ti–Mo [27,28], Co–Cr–Fe–Ni–Cu–Al [29], and Cu–Ni–Co–Zn–Al–Ti [30], the tendency is different. Although they contain a variety of BCC, FCC, and HCP elements and first form simple BCC and/or FCC crystalline solid solution phases due to high entropy effect, prolonged milling causes these solid solution phases to transform into amorphous phase similar to the feature of type I amorphization. Then, what would happen if the HEA system is only composed of HCP elements? To find this, the present work designed two equimolar alloys, BeCoMgTi and BeCoMgTiZn, and investigated the phase evolution from the elemental blended state to the final state in mechanical milling.

2. Experimental procedures

From the known 15 metallic elements with HCP structure at room temperature, five common elements, Be, Co, Mg, Ti, and Zn, with high purities (>99.9%) were chosen to generate the equimolar quaternary BeCoMgTi and quinary BeCoMgTiZn alloys (both expressed in molar ratio) by MA process. Table 1 [31] lists their fundamental properties. It can be seen that they have wide ranges of atomic size from 1.13 to 1.60 Å and melting point from 649 to 1660 °C. The mechanical milling was carried out by a SPEX 8000 vibration ball milling machine in a hardened SKD 11 steel vial sealed with an Ar atmosphere. The ball-to-powder weight ratio was 10:1. To avoid significant temperature rise, the steel vials were cooled by a continuous air flow during mechanical milling, and an interval of 10 min was periodically applied after each milling period of 30 min. The crystal structure evolution of the mixed powders with different milling times is examined by X-ray diffraction (XRD) with Shimadzu XRD-6000. A transmission electron microscope (TEM) modeled JEOL-2010 with energy dispersion spectrum (EDS) was used to investigate the final amorphous phase. Furthermore, an electron probe X-ray microanalyzer (EPMA) modeled JEOL JXA-8500F was used to analyze the distribution of elements in a milled powder particle.

3. Results and discussion

3.1. Phase evolution during MA

Fig. 1 shows the XRD patterns of powders with different milling times. Patterns of the elemental blend of BeCoMgTi and BeCoMgTiZn alloys, *i.e.* 0 h, show up all elemental peaks with a clean background. For the BeCoMgTi alloy after milling for 6 h, as shown in Fig. 1(a), a broad peak appears in the range of $35^\circ < 2\theta < 50^\circ$ besides those elemental peaks from all components. As milling time increases, peak intensities of pure elements decrease but intensity of the amorphous broad peak increases simultaneously. Finally, the alloy powder almost became fully amorphous with a broader peak in the range of $30^\circ < 2\theta < 55^\circ$ after milling for 144 h. A similar phenomenon is found in XRD patterns of the BeCoMgTiZn alloy powders as shown in Fig. 1(b). Elemental peaks become quite weak after milling for 72 h and the powder becomes fully amorphous with a broader peak in the range of $30^\circ < 2\theta < 55^\circ$ after milling for 144 h. However, the patterns show the quinary alloy takes a faster amorphization rate than the quaternary alloy in view of the relative height between elemental peaks and amorphous broad peak.

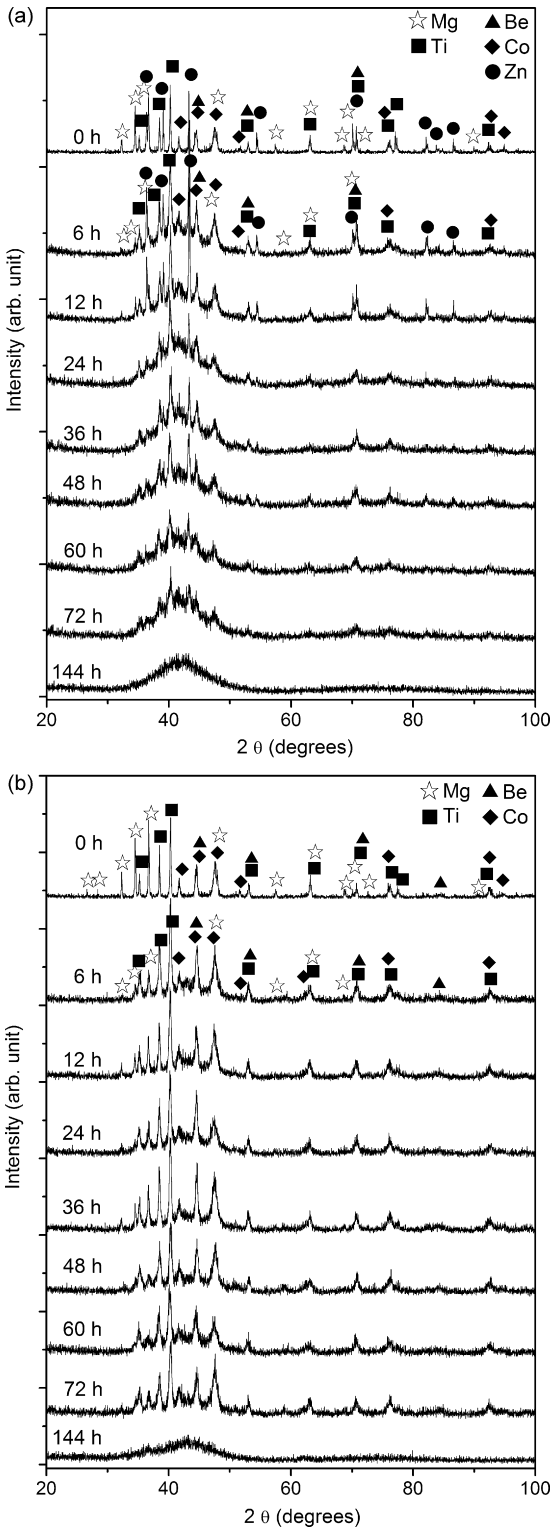

Fig. 1. XRD patterns of alloy powders milled with different times: (a) BeCoMgTi alloy and (b) BeCoMgTiZn alloy.

The amorphous powders were then examined by TEM. Fig. 2 shows TEM results of 144 h-milled BeCoMgTi alloy powder. The bright field image reveals no microstructural but only thickness contrast, as shown in Fig. 2(a), while the diffraction pattern shows an apparent diffuse ring which is attributed to amorphous structure. The dark field image, as shown in Fig. 2(b), obtained by selecting a part of the amorphous diffuse ring exhibits that the whole region becomes bright and has lots of white dots smaller than 1 nm dispersed throughout its matrix. Similar results were also obtained from the TEM observation of the 144 h-milled BeCoMgTiZn alloy powder as shown in Fig. 3. All these results confirm that the 144 h-milled particles have a homogeneous amorphous structure with short-range-order clusters smaller than 1 nm.

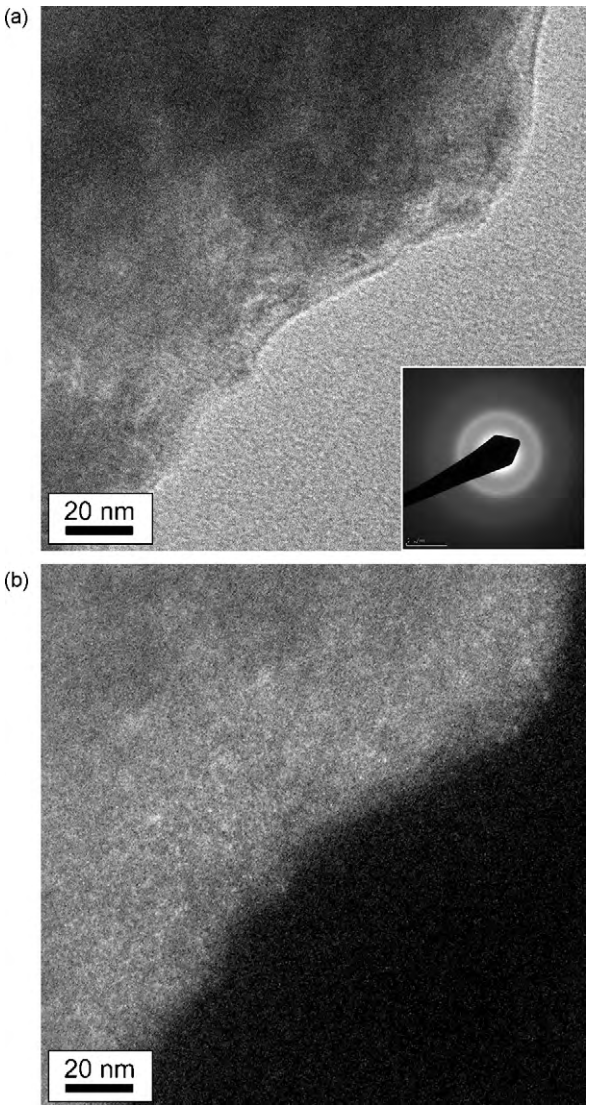

Fig. 2. TEM images of 144 h-milled BeCoMgTi alloy powder: (a) bright field image with diffraction pattern and (b) dark field image.

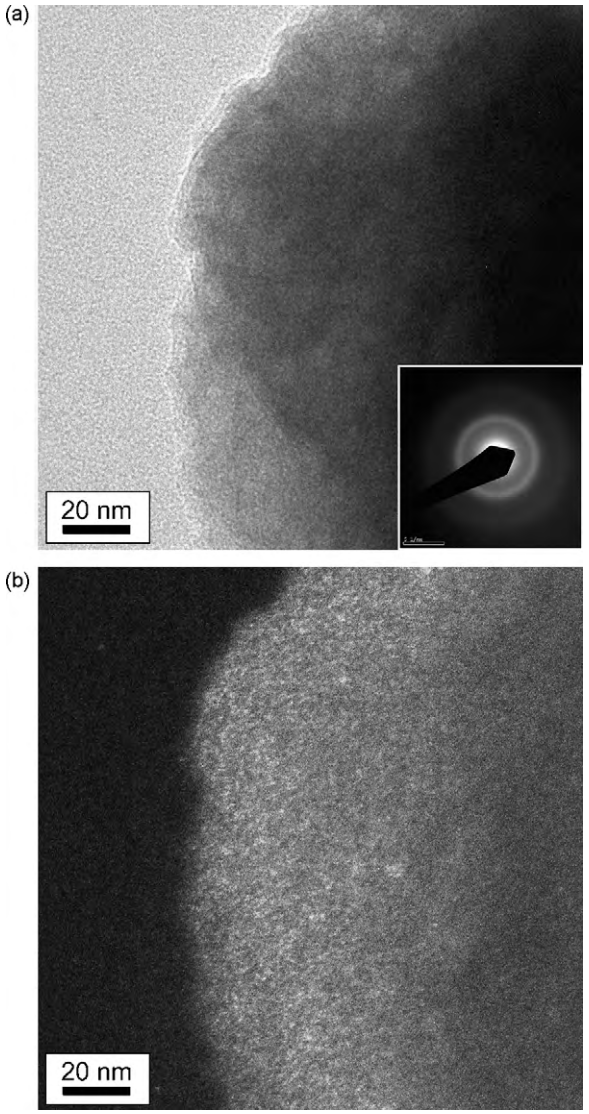

Fig. 3. TEM images of 144 h-milled BeCoMgTiZn alloy powder: (a) bright field image with diffraction pattern and (b) dark field image.

3.2. Amorphization type

By examining the evolution of XRD patterns in Fig. 1, it is apparent that the decrease of elemental peaks only associates with the increase of amorphous broad peaks. This illustrates that no crystalline solid solutions or intermetallic compounds form during the MA process. Consequently, both of them fit the features of type II amorphization proposed by Weeber and Bakker as mentioned in Section 1 [4]. Since the present alloys have equimolar components as HEAs, the mechanism of amorphization may be quite different from those multi-component alloys based on one principal element as given in Section 1 [5–10]. However, the amorphization type of the present system is also different from the type I amorphization found in the Cu–Ni–Al–Co–Cr–Fe–Ti–Mo HEA [28] which formed FCC solid solution phases prior to amorphization. It has been found that the FCC solid solution phase is mainly composed of Cu, Ni, Al, and Co having lower melting points and good chemical compatibility with each other. With prolonged milling, the FCC phase gradually dissolves other elements of higher melting points and finally transforms into an amorphous structure with the introduction of more defects and distortions.

3.3. Factors to determine amorphization type

In the amorphization of metallic glasses processed from liquid-to-solid, some famous rules such as Egami's rule [32] and Inoue's rules [33] have been proposed. In addition, the eutectic effect is very important to account for such an amorphization [12]. This is mainly due to that the supercooling to the glass temperature before forming detectable nucleation is easier to be achieved for the deep eutectic or near eutectic composition. However, MA is of solid-state reaction which is highly related to diffusion process (diffusion rate is also related to the melting point of elements) and assisted by severe deformation. Thus, the amorphization of MA is attributable to the effects of the crystal structure, atomic size, bonding energy, and melting point.

Table 2 [34,35] lists the bonding energies of unlike atom pairs in the present two alloys. The energies range from +16 to −30 kJ/mole. The Mg–Ti pair has moderate positive energy while other pairs have moderate negative or small positive energies. Without large positive or negative bonding energies, the strong repulsion or attraction between unlike atoms could be effectively prevented. Thus the formation of a mixed solid solution becomes favored instead of immiscible elemental clusters and intermetallic compounds. In

Table 2
Bonding energies of the possible unlike atom pairs (kJ/mole) [34,35].

Elements	Be	Co	Mg	Ti	Zn
Be	0	−4	−3	−30	4
Co	−4	0	3	−28	−5
Mg	−3	3	0	16	−4
Ti	−30	−28	16	0	−15
Zn	4	−5	−4	−15	0

milling the blended elemental power of BeCoMgTi alloy, Mg with the lowest melting point is the easiest one to deform, disintegrate and spread than more rigid Be, Co, and Ti with much higher melting point. This argument can be confirmed by the observation of EPMA color mapping of powders with different milling times as shown in Fig. 4. Although Be has weaker signal than Co and Ti due to the limitation of instrument, it can be noticed from the mapping of 60 h-milled powder, Fig. 4(a), that Mg spread more widely than other three elements and dissolve a significant amount of these elements in its matrix. It still can be seen that these three more rigid elements have more localized enriched regions than Mg since some of which even have red-color core indicating near 100% concentration. After prolonged milling as 144 h, the distribution of every element becomes uniform as shown in Fig. 4(b). Thus we can suggest that the dissolutions of disintegrated Be, Co, and Ti particles into Mg through diffusion are favorable from the initial milling stage. This is because moderate repulsion between Mg and Ti atoms can be compromised by the attractions of Be–Co, Be–Ti, and Co–Ti giving the increase of the overall bonding and thus the decrease of free energy. This is further aided by high mixing entropy and deformed structure in increasing the mutual solubility among elements. However, due to the wide range of atomic size from 1.13 to 1.60 Å, the crystalline structure has large distortion and strain energy, and thus becomes topologically unstable as compared with

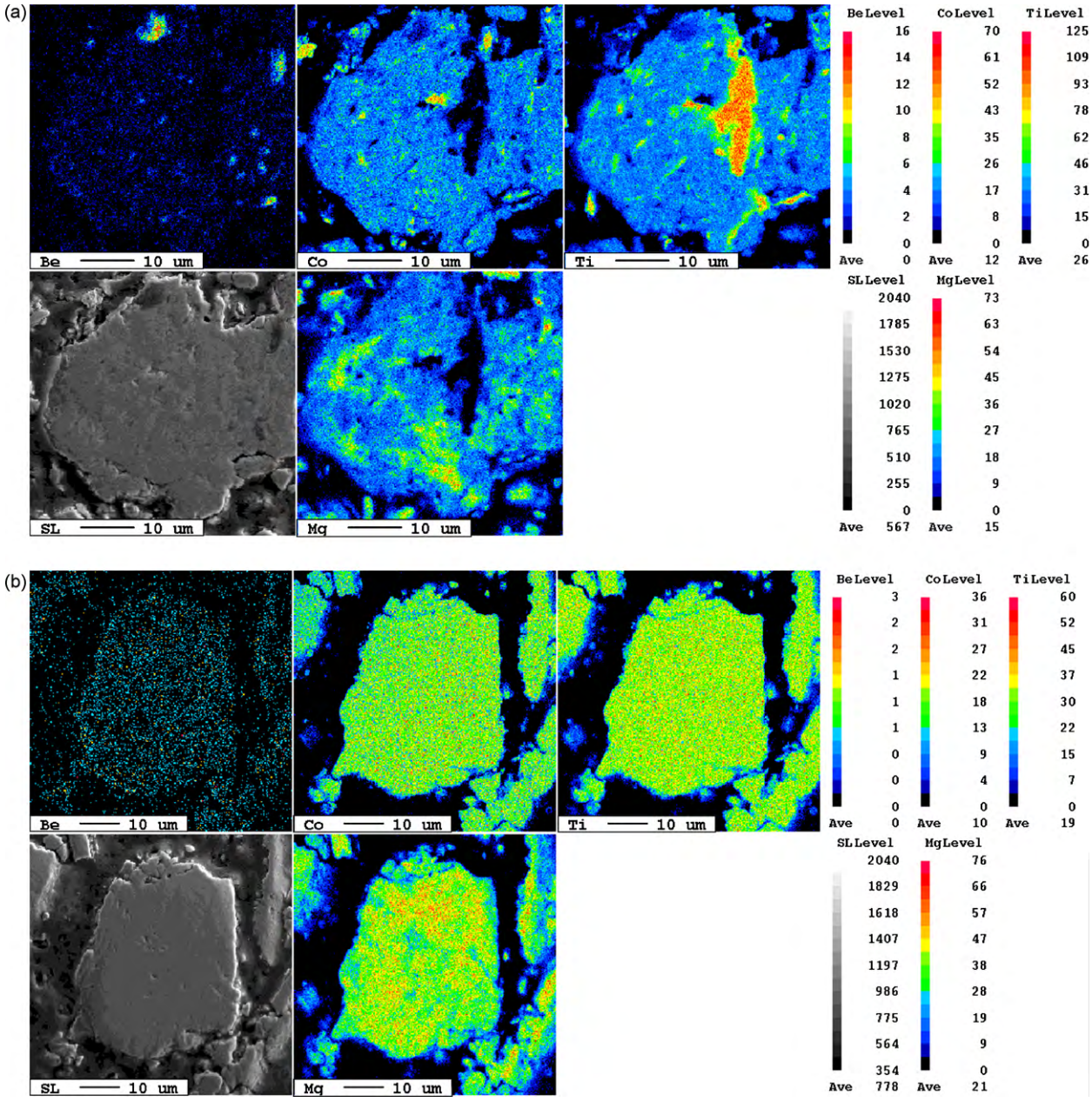

Fig. 4. EPMA color mappings of BeCoMgTi alloy powder with different milling times: (a) 60 h-milled and (b) 144 h-milled.

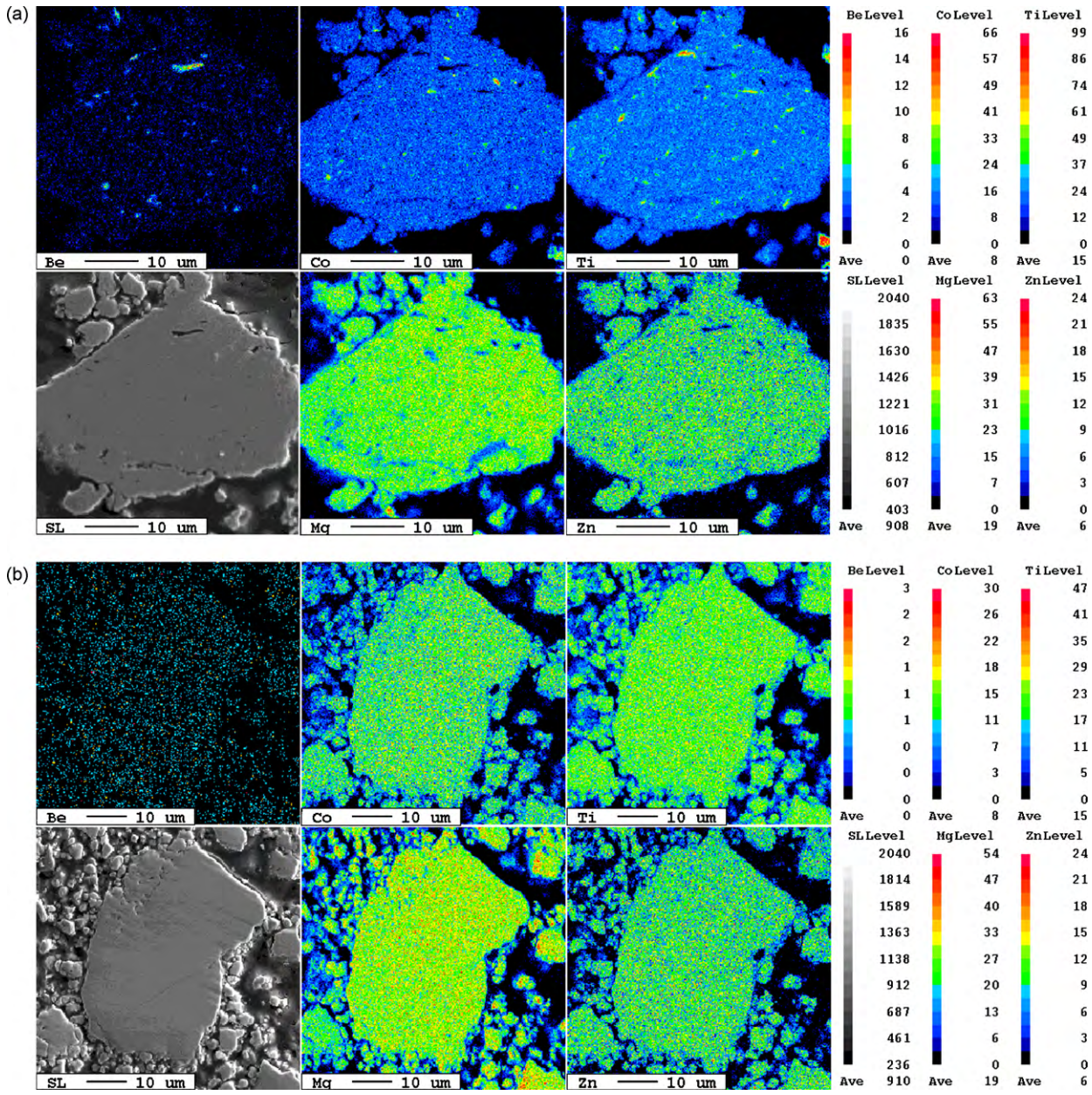

Fig. 5. EPMA color mappings of BeCoMgTiZn alloy powder with different milling times: (a) 60 h-milled and (b) 144 h-milled.

the amorphous structure in which strain energy is already released [32]. In fact, the size difference also fulfills the 12% size difference requirement of Inoue's rules [33] if Mg is regarded as the largest atom, Co and Ti medium-size atoms, and Be the smallest atom. This is why the amorphous phase forms from the initial milling stage as that of type II amorphization.

For the BeCoMgTiZn alloy displaying type II amorphization, the same mechanism discussed for BeCoMgTi alloy also holds true as Zn is again chemically compatible with the other four elements and fulfill the 12% size difference requirement of Inoue's rules [33] (see Tables 1 and 2). As for the observation that Fig. 1 shows incorporating Zn to enhance amorphization rate, the same mechanism explains that Zn having even lower melting temperature and better chemical attraction with Co and Ti than Mg (see Table 2) increases overall diffusion rate and solubility of the amorphous structure of BeCoMgTiZn [36]. This explanation conforms to the EPMA mapping of MA BeCoMgTiZn powders as shown in Fig. 5. In the 60 h-milled powder, Fig. 5(a), the mapping shows more uniform distribution of elements as compared with Fig. 4(a) although it also can be noticed that Be, Co, and Ti elements with high melting point still have small enriched spots in the particle. In the 144 h-milled powder, Fig. 5(b), the mapping shows fully uniform distribution of elements in the particles.

In contrast, the mechanism from the blended elemental state toward amorphization state is different from that of the Cu–Ni–Al–Co–Cr–Fe–Ti–Mo system mentioned in Section 3.2, as it is of type I amorphization [28]. This is because of the much smaller atomic size difference among Cu, Ni, Al, and Co atoms (atomic size varies from 1.25 to 1.43 Å) which constitute the initial FCC solution phase. Under this condition, lattice strain energy simply due to atomic size difference is not enough to let the crystalline structure topologically collapse into an amorphous structure [32]. The collapse requires more distortion and point defects achieved by dissolving more elements with prolonged milling. Therefore, there is some duration of crystalline FCC solid solution before amorphization in this system.

4. Conclusions

To summarize, this work prepared and investigated BeCoMgTi and BeCoMgTiZn equimolar alloys entirely composed of HCP elements by mechanical alloying. No crystalline solid solutions and compounds formed before full amorphization. The amorphization processes of these two alloys conform to type II amorphization of the classification proposed by Weeber and Bakker. The inhibition of intermetallic compounds before amorphization is due to chemical compatibility among the constituent elements in company with high entropy effect and deformation effect which enhance the mutual solubility. Direct formation of the amorphous solid solution phase instead of the crystalline one attributes to their large range of atomic size. This mechanism could be a guideline for type II amorphization of multi-component alloys.

References

[1] J.S. Benjamin, Metall. Trans. (1970) 2943–2951.
[2] D.L. Zhang, Prog. Mater. Sci. 49 (2004) 537–560.
[3] C. Suryanarayana, E. Ivanov, V.V. Boldyrev, Mater. Sci. Eng. A 304 (2001) 151–158.
[4] A.W. Weeber, H. Bakker, Phys. B 153 (1988) 93–135.
[5] M. Seidel, J. Eckert, L. Schultz, Mater. Lett. 23 (1995) 299–304.
[6] Z.G. Liu, J.T. Guo, Z.Q. Hu, J. Alloys Compd. 234 (1996) 106–110.
[7] B.S. Murty, M.M. Rao, S. Ranganathan, Scr. Metall. Mater. 24 (1990) 1819–1824.
[8] G.M. Dougherty, G.J. Shiflet, S.J. Poon, Acta Metall. 42 (1994) 2275–2283.
[9] K. Krivoroutchko, T. Kulik, H. Matyja, V.K. Portnoy, V.I. Fadeeva, J. Alloys Compd. 308 (2000) 230–236.
[10] S. Mula, S. Ghosh, S.K. Pabi, Mater. Sci. Eng. A 472 (2008) 208–213.
[11] J.W. Yeh, Ann. Chim. Sci. Mater. 31 (2006) 633–648.
[12] X.F. Wang, Y. Zhang, Y. Qiao, G.L. Chen, Intermetallics 15 (2007) 357–362.
[13] Y.F. Kao, T.J. Chen, S.K. Chen, J.W. Yeh, J. Alloys Compd. 488 (2009) 57–64.
[14] C.W. Tsai, Y.L. Chen, M.H. Tsai, J.W. Yeh, T.T. Shun, S.K. Chen, J. Alloys Compd. 486 (2009) 427–435.
[15] B. Ren, Z.X. Liu, D.M. Li, L. Shi, B. Cai, M.X. Wang, J. Alloys Compd. 493 (2010) 148–153.
[16] T.T. Shun, C.H. Hung, C.F. Lee, J. Alloys Compd. 495 (2010) 55–58.
[17] Y.L. Chen, Y.H. Hu, C.W. Tsai, J.W. Yeh, S.K. Chen, S.Y. Chang, Mater. Chem. Phys. 118 (2009) 354–361.
[18] V. Dolique, A.L. Thomann, P. Brault, Y. Tessier, P. Gillon, Surf. Coat. Technol. 204 (2010) 1989–1992.
[19] C.M. Lin, H.L. Tsai, J. Alloys Compd. 489 (2010) 30–35.
[20] C.Y. Hsu, T.S. Sheu, J.W. Yeh, S.K. Chen, Wear 268 (2010) 653–659.
[21] Y.F. Kao, T.D. Lee, S.K. Chen, Y.S. Chang, Corros. Sci. 52 (2010) 1026–1034.
[22] P.K. Huang, J.W. Yeh, Scr. Mater. 62 (2010) 105–108.
[23] M.I. Lin, M.H. Tsai, W.J. Shen, J.W. Yeh, Thin Solid Films 518 (2010) 2732–2737.
[24] M.H. Tsai, C.W. Wang, C.H. Lai, J.W. Yeh, J.Y. Gan, Appl. Phys. Lett. 92 (2008) (article number: 052109).
[25] S.Y. Chang, D.S. Chen, Appl. Phys. Lett. 94 (2009) (article number: 231909).
[26] S. Varalakshmi, M. Kamaraj, B.S. Murty, J. Alloys Compd. 460 (2008) 253–257.
[27] Y.L. Chen, Y.H. Hu, C.A. Hsieh, J.W. Yeh, S.K. Chen, J. Alloys Compd. 481 (2009) 768–775.
[28] Y.L. Chen, Y.H. Hu, C.W. Tsai, C.A. Hsieh, S.W. Kao, J.W. Yeh, T.S. Chin, S.K. Chen, J. Alloys Compd. 477 (2009) 696–705.
[29] K.B. Zhang, Z.Y. Fu, J.Y. Zhang, J. Shi, W.M. Wang, H. Wang, Y.C. Wang, Q.J. Zhang, J. Alloys Compd. 485 (2009) L31–L34.
[30] S. Varalakshmi, M. Kamaraj, B.S. Murty, Mater. Sci. Eng. A 527 (2010) 1027–1030.
[31] C. Kittel, Introduction to Solid State Physics, 7th ed., John Wiley & Sons, Inc., New York, 1996.
[32] T. Egami, Mater. Sci. Eng. A 226 (1997) 261–267.
[33] A. Inoue, T. Zhang, T. Masumoto, J. Non-Cryst. Solids 156 (1993) 473–480.
[34] F.R. de Boer, R. Boom, W.C.M. Mattens, A.R. Miedema, A.K. Niessen, Cohesion in Metals, 1st ed., Elsevier Scientific Pub. Co., New York, 1988.
[35] A. Takeuchi, A. Inoue, Mater. Trans. 46 (2005) 2817–2829.
[36] D.A. Porter, K.E. Easterling, Phase Transformations in Metals and Alloys, Chapman & Hall, London, 1992, pp. 75–91.